

# An energy-frequency parameter for earthquake ground motion intensity measure

Guan Chen<sup>1</sup>  | Jiashu Yang<sup>2</sup> | Yong Liu<sup>3</sup>  | Takeshi Kitahara<sup>4</sup>  | Michael Beer<sup>1,5,6</sup>

<sup>1</sup>Institute for Risk and Reliability, Leibniz Universität Hannover, Hannover, Germany

<sup>2</sup>State Key Laboratory of Disaster Reduction in Civil Engineering, College of Civil Engineering, Tongji University, Shanghai, P. R. China

<sup>3</sup>State Key Laboratory of Water Resources and Hydropower Engineering Science, Institute of Engineering Risk and Disaster Prevention, Wuhan University, Wuhan, P. R. China

<sup>4</sup>College of Science and Engineering, Kanto Gakuin University, Yokohama, Japan

<sup>5</sup>Institute for Risk and Uncertainty and School of Engineering, University of Liverpool, Liverpool, UK

<sup>6</sup>International Joint Research Center for Resilient Infrastructure & International Joint Research Center for Engineering Reliability and Stochastic Mechanics, Tongji University, Shanghai, P. R. China

## Correspondence

Guan Chen, Institute for Risk and Reliability, Leibniz Universität Hannover, 30167 Hannover, Germany.

Email: [guan.chen@irz.uni-hannover.de](mailto:guan.chen@irz.uni-hannover.de)

## Funding information

International Joint Research Platform Seed Fund Program of Wuhan University, Grant/Award Number: (Grant No. WHUZZJJ202207); National Natural Science Foundation of China, Grant/Award Number: (Grant No. 52079099)

## Abstract

A novel scalar ground motion intensity measure (IM), termed the energy-frequency parameter, is proposed based on the Hilbert-Huang transform. To validate the effectiveness of the proposed IM, the correlation analysis between the engineering demand parameter (EDP) and energy-frequency parameter is performed using 1992 recorded ground motions, in which EDP is the maximum inter-storey drift of structures obtained by nonlinear time-history analysis. Results show that the energy-frequency parameter has a strong linear correlation with EDP at natural logarithm, and this correlation is applicable for various structural fundamental periods. We also verified that the lognormal cumulative distribution function can characterize the energy-frequency parameter-based fragility function, which can further facilitate the application of the parameter in seismic risk analysis. Besides, the strong correlation between the energy-frequency parameter and other IMs (such as PGA, PGV, PGD, CAV,  $I_a$ ,  $v_{rms}$ , and SI) potentially makes the proposed IM widely applicable in seismic risk analysis. Moreover, since the energy-frequency parameter depends only on the frequency-domain characteristics of the ground-motion signal, it may closely link to seismological theory and provide new insights into seismology engineering.

## KEYWORDS

seismic risk analysis, ground motion IM, energy-frequency, Hilbert-Huang transform, fragility function

This is an open access article under the terms of the [Creative Commons Attribution-NonCommercial-NoDerivs](https://creativecommons.org/licenses/by-nc-nd/4.0/) License, which permits use and distribution in any medium, provided the original work is properly cited, the use is non-commercial and no modifications or adaptations are made.

© 2022 The Authors. *Earthquake Engineering & Structural Dynamics* published by John Wiley & Sons Ltd.

## 1 | INTRODUCTION

Seismic risk analysis, as a common method to study the adverse consequences of earthquakes, involves several aspects, such as earthquake occurrence, site response, ground motion characteristics, structural response, and consequence to structure. For example, performance-based earthquake engineering (PBEE), as a specific framework of seismic risk analysis, includes four phases (i.e., hazard analysis, structural analysis, damage analysis, and loss analysis) and refers to four variables (i.e., IM, engineering demand parameter [EDP], damage measure, and decision variable).<sup>1,2</sup> The ground motion IM, as the initial parameter that links the hazard analysis and structural analysis, is crucial for seismic risk analysis (see Rodgers et al.<sup>3</sup> and Park et al.<sup>4</sup>). In general, an ideal IM should be able to correlate seismological parameters with EDP effectively.

So far, various ground motion IMs have been proposed, such as peak ground acceleration (PGA), Arias intensity ( $I_a$ ), cumulative absolute velocity (CAV), root-mean-square of acceleration ( $a_{rms}$ ), acceleration spectrum intensity (ASI), and spectral acceleration at the fundamental period of the structure ( $S_a(T_1)$ ). The classifications of these IMs vary in different studies. For example,  $I_a$  and  $a_{rms}$  are viewed as duration-based IMs in De Biasio et al.,<sup>5</sup> but as energy parameters in Danciu and Tselentis.<sup>6</sup> In the present study, we divide the IMs into three categories, that is, amplitude-based, duration-based, and frequency-based IMs. Specifically, the amplitude-based IMs are tied to the time-domain amplitude of the ground motion, like PGA, CAV,  $I_a$ , and  $a_{rms}$ . The duration-based IMs mainly means uniformed duration,<sup>7</sup> significant duration,<sup>8</sup> and effective duration.<sup>9</sup> The frequency-based IMs are further divided into response spectra-based and frequency content-based IMs. The former is connected to the maximum linear structural response of the single-degree-of-freedom system subjected to ground motions, such as  $S_a(T_1)$ ,  $S_v(T_1)$ , ASI, and  $T_o$ . The latter depends on the ground motion frequency-domain properties after time-frequency conversion, like mean period ( $T_m$ ).<sup>10</sup> Additionally, when the IMs (like CAV and ASI) are the outcome of integration or cumulative, they are also regarded as energy parameters. For example, Arias intensity, as an amplitude-based IM, is also treated as an energy parameter because it is the integration of the acceleration. Details of the IMs used in this study are listed in Table 1.

The characterization and applicability of the ground motion IMs are discussed. The PGA, PGV, PGD, and duration-based IMs (like  $D_{s5-75}$  and  $D_{s5-95}$ ) are straightforward but relatively weakly correlated to EDPs, especially for systems

TABLE 1 Ground motion intensity measures used in this study

Category	IM	Definition	Remark
Duration-based IMs	$D_s$	Significant duration, <sup>8</sup> like $D_{s5-75}$ and $D_{s5-95}$	-
Amplitude-based IMs	PGA	Peak ground acceleration	-
	PGV	Peak ground velocity	-
	PGD	Peak ground displacement	-
	$I_a$	Arias intensity, <sup>11</sup> $I_a = \frac{\pi}{2g} \int_0^t a^2(t)dt$	Energy parameter
	CAV	Cumulative absolute velocity, <sup>12</sup> $CAV = \int_0^t  a(t) dt$	Energy parameter
	CAD	Cumulative absolute displacement, <sup>12</sup> $CAD = \int_0^t  v(t) dt$	Energy parameter
	$a_{rms}$	Root-mean-square of acceleration, <sup>13</sup> $a_{rms} = \sqrt{\frac{1}{t} \int_0^t a^2(t)dt}$	Energy parameter
	$v_{rms}$	Root-mean-square of velocity, <sup>13</sup> $v_{rms} = \sqrt{\frac{1}{t} \int_0^t v^2(t)dt}$	Energy parameter
Frequency-based IMs	$d_{rms}$	Root-mean-square of displacement, <sup>13</sup> $d_{rms} = \sqrt{\frac{1}{t} \int_0^t d^2(t)dt}$	Energy parameter
	$S_a(T)$	Spectral acceleration at $T$ s	-
	$T_m$	Mean period <sup>10</sup>	-
	$T_o$	Smooth spectral period <sup>14</sup>	-
	$T_{avg}$	Average spectral period <sup>14</sup>	-
	$T_g$	Characteristics period <sup>15</sup>	-
	ASI	Acceleration spectrum intensity <sup>16</sup> , $ASI = \int_{0.1}^{0.5} S_a(\xi = 5\%, T)dT$	Energy parameter
SI	Spectrum intensity <sup>17</sup> , $SI = \int_{0.1}^{2.5} S_{pv}(\xi = 5\%, T)dT$	Energy parameter	

involving various fundamental structural periods. For example, Yang et al.<sup>15</sup> pointed out that PGA is closely correlated to the structure with the shorter fundamental structural period, but not the optimal IM for structure with a longer fundamental structural period. The ground motion duration is also verified to have influences on structural responses.<sup>18,19</sup> However, the relationship between duration-based IMs and EDPs is not significant. In contrast, the spectral acceleration at fundamental period ( $S_a(T_1)$ ), as the most popular response spectra-based IM, is widely utilized in seismic risk analysis due to their strong correlation to the EDPs.<sup>20,21</sup> Many studies are also carried out to further improve the effectiveness of  $S_a(T_1)$ . Bojórquez and Iervolino<sup>22</sup> proposed a parameter to describe the shape of response spectra. Baker and Cornell<sup>23</sup> shared a vector IM, which combines the  $S_a(T_1)$  and the epsilon between spectral acceleration of record and the mean of ground motion prediction equation at the given period, to improve the prediction accuracy of structural behavior. Kohrangi et al.<sup>24</sup> considered the second vibration mode and spectral shape of the response spectrum. However, the response spectrum-based parameters are relatively less related to the seismological parameters than the frequency content-based IMs.<sup>25</sup> On the other hand, the mean period ( $T_m$ ),<sup>10</sup> which is determined by the Fourier frequency amplitude characteristics, is strongly connected to the seismological parameter, but less correlated to the EDPs. Hence, the IM simultaneously correlated to both seismological parameters and EDPs remains challenging.

Energy parameters, as cumulative measures, have been demonstrated to be strongly related to EDPs in seismic hazard analysis because it considers the amplitude, frequency, and duration of ground motion.<sup>26,27</sup> For example, structure-specific energy parameters, such as absolute input energy,<sup>28</sup> the total dissipated energy,<sup>29</sup> and referential energy,<sup>30</sup> are confirmed as useful indices in predicting the structural behavior.<sup>31</sup> The non-structure-specific energy parameters related to ground motion amplitude (such as  $I_a$ , CAV, and  $a_{rms}$ ) and response spectrum (such as ASI and SI) are also widely used as IMs in seismic hazard and risk analysis.<sup>32,33</sup> These studies significantly facilitate the seismic risk analysis. However, compared with the sufficient research on amplitude- and response spectrum-based energy parameters, the frequency content-based energy parameters are less studied.

Therefore, this study proposed a novel frequency content-based IM based on Hilbert-Huang transform (HHT), termed energy-frequency parameter, and verified that the parameter is strongly correlated to the EDP using 1992 recorded ground motions in the Pacific Earthquake Engineering Research (PEER) database, in which EDP is the maximum inter-storey drift of structures obtained by nonlinear time-history analysis with the OpenSees finite element software. Moreover, compared to other IMs that generally require special modification for near-fault pulse-like ground motion in seismic risk analysis (e.g., Yang et al.<sup>15</sup> and Tothong and Cornell<sup>34</sup>), the energy-frequency parameter is applicable for both pulse-like and ordinary ground motion. Besides, the energy-frequency parameter-based fragility function can be characterized by a lognormal cumulative distribution function (CDF), which would further help to facilitate the application of the parameter in seismic risk analysis. Apart from the advantage of the strong correlation with EDP, the energy-frequency parameter potentially provides new insights into seismology engineering because the parameter is only based on the ground-motion signal without involving structural response procedures.<sup>25</sup> The correlation analysis between the energy-frequency parameter and other popular IMs is also discussed.

## 2 | DEFINITION OF ENERGY-FREQUENCY PARAMETER

A scalar energy-frequency parameter is proposed for ground motion IM and defined in Equation (1).

$$h = \sum_i E(f_i) \frac{1}{f_i} \quad (0.3/\alpha \leq f_i \leq 15 \text{ Hz}, \Delta f \leq 0.05 \text{ Hz}) \quad (1)$$

where  $h$  is the energy-frequency parameter for ground motion acceleration;  $E(f_i)$  is the energy at the frequency  $f_i$ , in which  $f_i = f_s + i\Delta f$  ( $i = 0, 1, 2, \dots, N$ ) and  $\Delta f$  is the frequency interval;  $\alpha$  is a parameter for determining the starting frequency  $f_s$ . When the study involves to a specific structure,  $\alpha$  is recommended to agree with the fundamental period of the structure. Otherwise,  $\alpha$  is recommended to be 6, that is  $f_s = 0.05$  Hz. Besides, an interesting point is that the dimension of the proposed energy-frequency parameters agrees with Planck constant, that is,  $\text{ML}^2\text{T}^{-1}$ .

To obtain the frequency-domain energy, the time-frequency conversion for the signal is first required. The HHT is recommended herein. The reasons for applying HHT instead of other time-frequency conversion methods, such as Fourier

transform and wavelet transform, and for using of the summation range and frequency resolution of Equation (1) are discussed in Section 4.2.

HHT performs time-frequency analysis by integrating the empirical mode decomposition (EMD) and Hilbert transform.<sup>35</sup> For a signal  $S(x)$ , it can be expressed in Equation (2) based on DEM.

$$S(x) = \sum_{i=1}^n c_i + r_n \quad (2)$$

where  $c_i$  is the intrinsic mode function (IMF);  $r_n$  is the residue.

On the other hand, the analytic signal  $\zeta(t)$  of signal  $x(t)$  is defined in Equation (3) based on the Hilbert transform.

$$\zeta(t) = x(t) + j\tilde{x}(t) = a(t)e^{j\theta(t)} \quad (3)$$

$$\tilde{x}(t) = x(t) * \frac{1}{\pi t} = \frac{1}{\pi} \int_{-\infty}^{+\infty} \frac{x(\tau)}{t - \tau} d\tau \quad (4)$$

where  $j = \sqrt{-1}$ ; \* represents convolution;  $\tilde{x}(t)$  denotes the Hilbert transform of  $x(t)$ ;  $a(t)$  and  $\theta(t)$  are the instantaneous amplitude and the phase, and can be calculated by Equation (5) and Equation (6), respectively.

$$a(t) = \sqrt{x^2(t) + \tilde{x}^2(t)} \quad (5)$$

$$\theta(t) = \tan^{-1} \frac{\tilde{x}(t)}{x(t)} \quad (6)$$

The instantaneous frequency  $\omega$  is expressed in Equation (7).

$$\omega = -\frac{d\theta}{dt} \quad (7)$$

After performing Hilbert transform on each IMF, the original signal can be expressed as the real part of the analytic signal, as shown in Equation (8), where the residue part is ignored.

$$S(x) = \text{Re} \left\{ \sum_{j=1}^n a_j(t) e^{-i \int \omega_j(t) dt} \right\} = H(\omega, t) \quad (8)$$

where  $\text{Re}\{\cdot\}$  present the real part of a complex signal;  $H(\omega, t)$  is the Hilbert spectrum.

The Hilbert marginal spectrum  $\hbar(\omega)$  is defined in Equation (9).

$$\hbar(\omega) = \int_0^{t_d} H(\omega, t) dt \quad (9)$$

where  $t_d$  is the duration of the signal.

The HHT frequency-domain energy  $E(\omega_i)$  is defined in Equation (10).

$$E(\omega_i) = |\hbar(\omega_i)|^2 \quad (10)$$

where  $E(\omega_i)$  is the energy at frequency  $\omega_i$ .

The normalized cumulative energy distribution  $C_r$  is expressed in Equation (11).

$$C_r = \frac{\sum_{i=1}^r E_i}{\sum_{i=1}^n E_i} \quad (11)$$

### 3 | VERIFICATION OF EFFECTIVENESS

#### 3.1 | Ground motion database

The proposed energy-frequency parameter is verified using ground motions from three earthquakes in PEER NGA-West2 database,<sup>36</sup> namely Imperial Valley-06 earthquake, Chi-Chi, Taiwan earthquake, and EI Mayor-Cucapah earthquake. The earthquake magnitude and hypocenter depth of Imperial Valley-06 earthquake are 6.53 Mw and 9.96 km, respectively, those of Chi-Chi, Taiwan earthquake are 7.62 Mw and 8 km, respectively, and those of EI Mayor-Cucapah earthquake are 7.2 Mw and 5.5 km, respectively. The number of ground motions records (including two horizontal and one vertical direction) in Imperial Valley-06, and Chi-Chi, Taiwan, and EI Mayor-Cucapah earthquake are 96, 1194, and 702, respectively.

Since the pulse-like ground motions tend to cause severer damage to structures than ordinary ground motions (see Chen et al.<sup>37</sup> and Phan et al.<sup>38</sup>), and the IM of pulse like ground motion generally requires particular modification (see Kohrangi et al.<sup>24</sup> and Tothong and Cornell<sup>34</sup>), the energy-frequency parameter of pulse-like and non-like ground motions are separately investigated to test the applicability of the proposed IM. The Imperial Valley-06 and Chi-Chi, Taiwan earthquakes, as two typical near-fault earthquakes, are used as databases for pulse-like ground motions. Based on the identification method of pulse-like ground motions,<sup>39</sup> the data volume of pulse-like and non-pulse ground motions in Imperial Valley-06 earthquake are 31 and 65, respectively, and in Chi-Chi, Taiwan earthquake are 157 and 1037, respectively. The identification method is a generalized continuous wavelet transform (CWT) method by combining convolution analysis with evaluation parameters. This method is based on the classical CWT identification method in Baker,<sup>40</sup> but overcomes the limitations of the classical CWT method that requires a wavelet basis and provides a workable and flexible framework for pulse-like ground motion identification. Specifically, the ground-motion velocity, which contains long-period and high-amplitude pulse and PGV is greater than 30 cm/s, is regarded as pulse-like ground motion in the method. More information of pulse-like ground motions, such as pulse period and pulse energy, can be found in Chen et al.<sup>39</sup>

#### 3.2 | Structural model

In order to demonstrate the applicability and effectiveness of the proposed energy-frequency parameter, verification calculations are carried out by modeling typical building structures according to the Code For Seismic Design of Buildings (GB 50011-2010) in China. In particular, five 3D nonlinear frame structures of different materials and heights are considered. In this manner, the verification calculations can cover structures of diverse vibration properties, and consequently, more insights into the proposed parameter can be presented.

All these structures are modeled based on the OpenSees platform using displacement-based nonlinear beam-column elements. To describe the nonlinearity of the concrete material, a uniaxial Kent-Scott-Park model<sup>41</sup> with degraded linear unloading/reloading stiffness and no tensile strength<sup>12</sup> is adopted. In addition, a uniaxial bilinear model with kinematic hardening is adopted to characterize the nonlinearity in both rebars and steel members.

In the concrete frame structures, the compressive strength and the crushing strength of the concrete material are 26.8 and 10 MPa, respectively. The concrete strains at the compressive strength and the crushing strength are taken as 0.002 and 0.0033, respectively. Besides, the elastic modulus, yield strength, and strain-hardening ratio of rebars equal 20 GPa, 335 MPa, and 0.001, respectively. For the steel frame structures, the elastic modulus, yield strength, and strain-hardening ratio of steel material are 20GPa, 235MPa and 0.01, respectively. The damping ratio of the first two modes of concrete and steel structures are assumed to be 0.05 and 0.03, respectively. Moreover, live loads are considered in the form of nonstructural masses.

Some other important parameters for five models that have different fundamental structural periods ( $T = 0.3, 0.6, 1, 3, 5$  s) are given as follows, respectively. The diagrams of the considered structures are shown in Figure 1.

1.  $T = 0.3$  s. This structure is a two-story reinforced concrete frame structure, as shown in Figure 1A. The structure consists of one and two bays along the X and Y directions, respectively. Both the height of each floor and the width of each bay are 4.50 m. The finite element model includes 18 nodes and 26 3D nonlinear beam-column elements. The accurate fundamental period of this structure is 0.34 s.



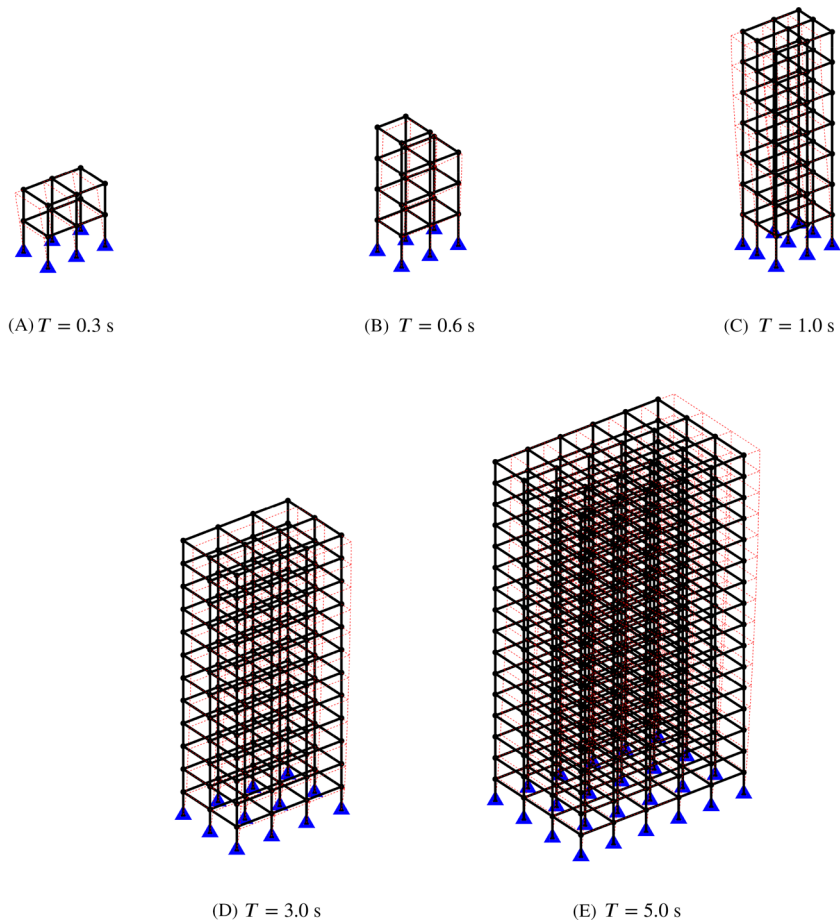


**FIGURE 1** Diagrams of the five frame structures. Solid lines present the structural members; the dashed lines present the first mode of the structure; the triangle marks denote fixed supports.

2.  $T = 0.6$  s. This structure is a four-story reinforced concrete frame structure, which is shown in Figure 1B. There is one bay along the X direction and two bays along the Y direction. Both the height of each floor and the width of each bay are 4.50 m. The finite element model are established with 28 nodes and 47 elements. The accurate fundamental period of this structure is equal to 0.57 s.
3.  $T = 1$  s. This structure is a seven-story reinforced concrete frame structure, of which the floor height is 4.50 m. As show in Figure 1C, the structure has two bays in both the X and Y directions, and the bay widths are 3.0 and 4.0 m, respectively. There are 72 nodes and 147 elements in the finite element model and the accurate fundamental period of the model equals to 0.97 s.
4.  $T = 3$  s. The steel frame structure shown in Figure 1D is taken as the testing structure for this case. The building has 12 floors with the same height equal to 3.66 m. The numbers of bays along the X and Y directions are two and three, respectively. In addition, the width of a bay is 6.10 m in both directions. Finally, 136 nodes and 348 elements are used to model the considered structure. The accurate fundamental period of this structure is equal to 3.07 s.
5.  $T = 5$  s. This structure is a steel frame structure with 16 stories, which is presented in Figure 1E. The heights of all stories are uniform and equal to 3.81 m. Besides, the structure has five and three bays along the X and Y directions, respectively. The widths of bays in the X and Y directions are 6.40 and 7.31 m, respectively. A total of 408 nodes and 992 beam–column elements are adopted to simulate the structure. The accurate fundamental period of this structure is 5.08 s.

The frame structures are subjected to unidirectional seismic excitation in this study. In particular, the seismic excitation is considered along the directions featured by translations of the first mode. Furthermore, to take into account the effect of slabs, rigid diaphragms are assumed in all the frame structures. Besides, to focus on the topic of this study that aims to propose a energy-frequency parameter and validate its effectiveness, only some important information of the structures is given herein. For more details of the structural models, such as the layout of standard floors, and the section sizes of columns and beams, the readers can refer to the Supporting Information (SI).

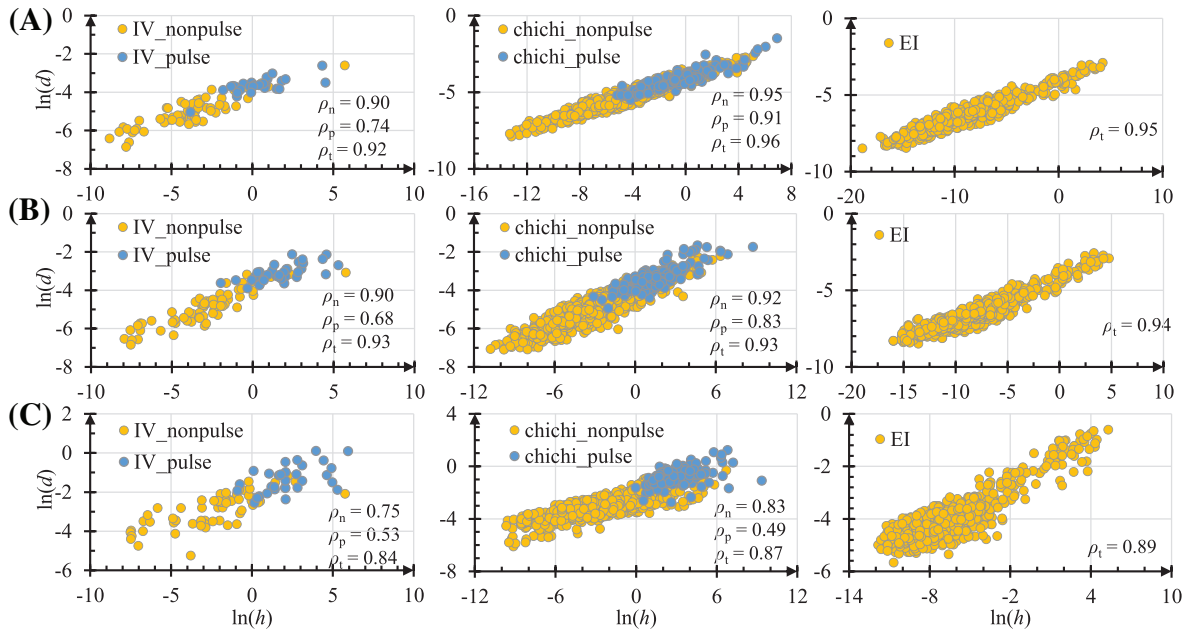


**FIGURE 2** Correlation analysis between energy-frequency parameter  $h$  and maximum inter-story drift  $d$  under different structure fundamental period  $T$ . (A)  $T = 0.3$  s; (B)  $T = 1$  s; (C)  $T = 5$  s.  $\rho_n$ ,  $\rho_p$ , and  $\rho_t$  are the Pearson correlation coefficients of non-pulse, pulse and total ground motions, respectively.

### 3.3 | Correlation analysis

The correlation analysis between ground motion IM and EDP is generally applied to evaluate the effectiveness of IM (e.g., De Biasio<sup>5</sup> and Luco and Cornell<sup>42</sup>). In this study, the energy-frequency parameter and maximum inter-story drift are employed as IM and DEP, respectively.

The relationship between the maximum inter-storey drift and energy-frequency parameter using the form of natural logarithm is plotted in Figure 2. Their Pearson correlation coefficient  $\rho$  (see Equation (12)) is also provided. Moreover, the pulse-like and non-pulse ground motions in Imperial Valley-06 and Chi-Chi, Taiwan earthquakes are separately investigated.

$$\rho = \frac{\sum(x_i - \bar{x})(y_i - \bar{y})}{\sqrt{\sum(x_i - \bar{x})^2 \sum(y_i - \bar{y})^2}} \quad (12)$$

where  $\rho$  denotes the Pearson correlation coefficient;  $x_i = \ln(h_i)$ , in which  $h_i$  is the energy-frequency parameter, and  $\ln(\cdot)$  represents natural logarithm;  $y_i = \ln(d_i)$ , and  $d_i$  is the maximum inter-storey drift;  $\bar{x}$  and  $\bar{y}$  are the mean values of  $x_i$  and  $y_i$ , respectively.

Figure 2 indicates that (a) the energy-frequency parameter has a strong positive correlation with the maximum inter-storey drift, and the applicability of the proposed IM is not limited by the fundamental structural period and seismic source of ground motion. (b) The energy-frequency parameters of pulse-like ground motions are generally larger than those of non-pulse ground motions, but the energy-frequency parameter cannot accurately classify the pulse-like and non-pulse ground motions due to the overlap regions. Besides, even if a study involves near-fault pulse-like ground motions, the energy-frequency parameter as IM remains appropriate and requires no extra modifications. (c) The correlation between the maximum inter-storey drift and energy-frequency parameter decreases with the increase of the fundamental structural period, which may be related to the fact that the significant periods of most of ground motions are low (generally below 2.0 s), where the significant period is the value corresponding to the maximum Fourier amplitude.

## 4 | DISCUSSION

### 4.1 | *h*-based fragility function

The seismic fragility function, as a core element of seismic probability risk analysis, describes the probability of a structure reaching or exceeding the damage state on the condition of ground motion IMs.<sup>43</sup> The fragility function can be expressed in Equation (13).

$$f_s = P[D \geq d_r | IM = x] \quad (13)$$

where  $f_s$  is the probability of failure;  $P[A|B]$  is the probability that  $A$  is true given than  $B$  is true;  $D$  is the EDP;  $d_r$  is the damage state;  $IM$  is the ground motion IM;  $x$  is a particular value of IM.

In this study, the energy-frequency parameter,  $h$ , is used as the IM, and the maximum inter-storey drift  $d$  is employed as the EDP. The limitation of inter-storey drift stipulated in Eurocode8 is utilized as the damage state and is expressed in Equation (14).

$$d_r \nu \leq 0.010H \quad (14)$$

where  $d_r$  is the maximum allowable inter-story drift;  $\nu$  is the reduction factor, which is related to the seismic hazard conditions and the protection of property objective, and is set to 0.5 herein;  $H$  is the storey height. That is, the structure would fail if the maximum inter-storey drift is greater than  $0.010H/0.5$ .

As shown in Figure 2, the energy-frequency parameter is strongly correlated to the maximum inter-storey drift. Their relationship can be expressed in a linear form as shown in Equation (15).<sup>44</sup>

$$\ln(d) = a \ln(h) + b + \epsilon \quad (15)$$

where  $a$  and  $b$  are the regression parameters;  $\epsilon$  is the residual, which is the difference between the computed and estimated logarithmic value of drift.

Using all ground motions in Imperial Valley-06, Chi-Chi Taiwan, and EI Mayor-Cucapah earthquakes, for a total of 1992 data, the regression relationships between energy-frequency parameter and inter-storey drift for five different fundamental structure periods (i.e.,  $T = 0.3, 0.5, 1, 3,$  and  $5$  s) are obtained based on the form in Equation (15), as shown in Figure 3A. The residual obeys a normal distribution according to the statistical analysis. An example of residual distribution is shown in Figure 3B, and more data are listed in Figure S4. The normal distribution parameters (mean value  $\mu$  and standard deviation  $\sigma$ ) for the residual at different fundamental periods are provided in the side table of Figure 3B.

Due to the residual obeying normal distribution, together with the additivity property of normal distribution,  $\ln(d)$  also obeys normal distribution. That is, the  $d$  obeys lognormal distribution, which agrees with the previous studies that often use the lognormal CDF to define the fragility function (e.g., Eads et al.<sup>45</sup> and Porter et al.<sup>46</sup>). Hence, the  $h$ -based fragility function can also be formulated by the CDF of the lognormal distribution. However, the CDF represents the probability of a value less than  $x$ , while the fragility function is the probability of a structure reaching or exceeding the damage state  $x$ . Hence, the  $h$ -based fragility function can be expressed in Equation (16). Based on this function, five fragility curves for the fundamental structural periods of 0.3, 0.5, 1, 3, and 5 s are provided in Figure 3C, respectively.

$$f_s = 1 - F(x; \mu, \sigma)$$

$$F(x; \mu, \sigma) = \frac{1}{\sqrt{2\pi}\sigma} \int_0^x \frac{1}{t} \exp\left(-\frac{(\ln(t) - \mu)^2}{2\sigma^2}\right) dt \quad (16)$$

where  $F(x; \mu, \sigma)$  is the CDF of lognormal distribution;  $x$  represents the maximum allowable inter-storey drift  $d_r$ . Based on the storey height of structural models in different fundamental structural periods, the maximum allowable drift for structure with fundamental period equaling to 0.3 s ( $d_r^{(0.3)}$ ), 0.6 s ( $d_r^{(0.6)}$ ), 1 s ( $d_r^{(1)}$ ), 3 s ( $d_r^{(3)}$ ) and 5 s ( $d_r^{(5)}$ ) is 0.090, 0.090, 0.090, 0.061, and 0.064 m using Equation (14), respectively.  $\mu$  and  $\sigma$  are the lognormal distribution parameters of the maximum inter-storey drift  $d$ , in which  $\mu$  can be calculated using the formulation in Figure 3A, and  $\sigma$  agrees with the standard deviation of residual in table of Figure 3B. For example, when the ground motion energy-frequency parameter  $h$  is 100,  $\mu$  is -2.99 based on the regression equation for the fundamental structural periods at 0.3 s, that is  $0.25 \times \ln(100) - 4.14$ ;



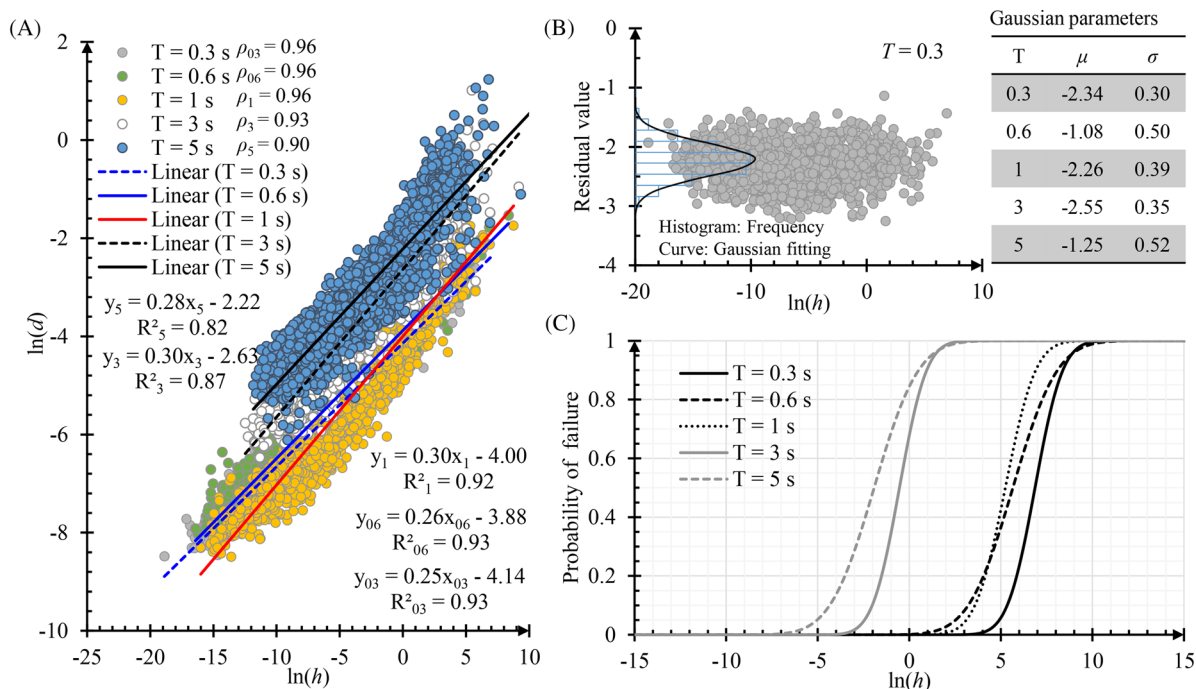


**FIGURE 3** (A) The regression analysis between energy-frequency parameter,  $h$ , and the maximum inter-storey drift  $d$  in natural logarithm. The Pearson correlation coefficient ( $\rho$ ) between  $\ln(h)$  and  $\ln(d)$  is also provided. In the regressive linear equation,  $x$  and  $y$  represents  $\ln(h)$  and  $\ln(d)$ , respectively, and  $R^2$  is the coefficient of determination. (B) An example for the scatter plots, frequency statistics (histogram), and Gaussian fitting (curve) of the residual in fundamental period  $T = 0.3$  s. The x-axis for histogram and curve is not plotted. The normal distribution parameters, the mean values  $\mu$  and the standard deviations  $\sigma$ , of the residuals in different fundamental periods  $T$  are listed in the side table. (C) The  $h$ -based fragility function for structures with different fundamental periods

the corresponding  $\sigma$  is 0.30; the maximum allowable inter-storey drift  $x$  is 0.09; and the probability for the maximum inter-storey drift ( $d$ ) over the maximum allowable value is 0.0262 by  $f_s = 1 - F(0.09; -2.99, 0.30)$ .

Therefore, the lognormal CDF is applicable for energy-frequency parameter based fragility function. This property can further facilitate the application of the parameter in seismic risk analysis. The fragility functions can be directly used in seismic risk analysis when it involves structures similar to structural model in Figure 1, and also provides a workable procedure to evaluate the structural response in engineering practice.

## 4.2 | Influencing factors for energy-frequency parameter

As defined in Equation (1), three factors, i.e., time-frequency conversion method, summation range ( $f_i$ ) and frequency resolution ( $\Delta f$ ), determine the value of energy-frequency parameter. To obtain the optimal energy-frequency parameter, the influences of these factors are discussed.

Apart from the HHT, Fourier transform (FT) (e.g., Li et al.<sup>47</sup>) and wavelet packet transform (WPT) (e.g., Chen et al.<sup>48</sup>) are also widely used in time-frequency analysis. The theory of FT and WPT in time-frequency conversion and frequency-domain energy calculation is introduced in SI. The related parameters of these methods in time-frequency conversion are set as follows: the wavelet basis and decomposition level of WPT is *sym5* and 11, respectively; the frequency resolution of HHT is 0.02 Hz. Examples for time-frequency conversion of ground motions based on FT, WPT, and HHT are shown in Figure 4A. It indicates that all the methods successfully convert the signal from time to frequency domain. However, HHT has greater resolution in the low-frequency region than FT and WPT, which helps reveal the impacts of ground motion on long fundamental period structures. More characteristics about FT, WPT, and HHT in time-frequency conversion are listed in SI, where the normalized cumulative energy distribution of all ground motions are plotted in Figure S3.

In addition, the Pearson correlation coefficient between the FT-, WPT-, and HHT-based energy-frequency parameter and maximum inter-storey drift (see Figure 4B) indicates that the performance of FT is inferior to WPT and HHT, and the performances of HHT and WPT are similar. However, the selection of wavelet basis and decomposition level is an annoying

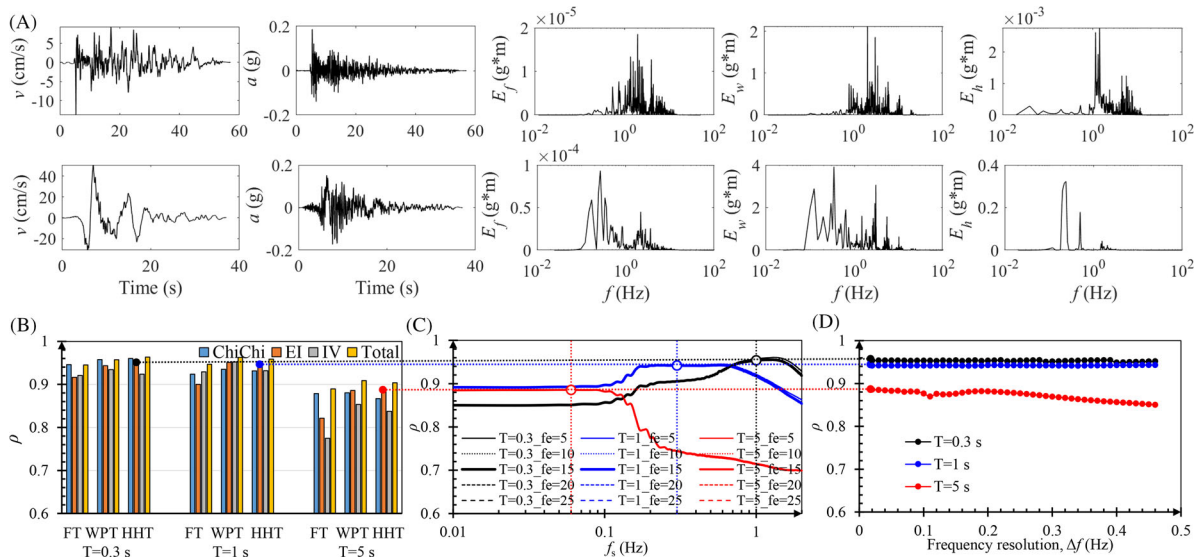


**FIGURE 4** Influencing factors on energy-frequency parameter. (A) Examples for velocity ( $v$ ), acceleration ( $a$ ), FT-based ( $E_f$ ), WPT-based ( $E_w$ ) and HHT-based ( $E_h$ ) frequency-domain energy distribution of non-pulse (upper, RSN 167 Horizontal 1) and pulse-like (below, RSN 174 Horizontal 1) ground motion in Imperial Valley-06 earthquake. (B) Pearson correlation coefficient between FT-, WPT-, and HHT-based energy-frequency parameters and maximum inter-story drift of structure with different fundamental period under Chi-Chi, Taiwan (chichi), EI Mayor-Cucapha (EI), Imperial Valley (IV) earthquake ground motions. The legend of ‘Total’ means all ground motions in three earthquakes are used. (C) and (D) investigates the effects of summation range and HHT frequency resolution on correlation coefficient, respectively, in which the EI Mayor-Cucapha earthquake ground motions are used. More data are provided in Figures S6 and S7

problem in WPT. The effects of wavelet basis and decomposition levels of WPT on correlation analysis are analyzed in Figure S5. On the contrary, HHT is an adaptive signal processing approach based on signal attributes, without determining the basis ahead. Therefore, because of the ability of high-resolution in low-frequency regions and the adaptive property, HHT is recommended herein.

The influences of summation range are also investigated from 0.01:0.01:2 Hz as the starting frequency ( $f_s$ ) to 5:5:25 Hz as ending frequency ( $f_e$ ). Results in Figure 4C show that the starting frequency has a significant impact on the correlation coefficient; however, the effects of the ending frequency are slight. This is because the reciprocal form of frequency is adopted in the definition, and consequently, the low-frequency regions mainly control the energy-frequency parameter. To accurately include the target frequency range that affects the structural response, this study suggests a starting frequency to be  $0.3/\alpha$ . If a specific structure is analyzed,  $\alpha$  is the fundamental structural period. In other words, the starting frequency is 0.3 times the fundamental structural frequency. The starting frequencies are always lower than fundamental structural frequency because the energy in the lower-frequency regions (i.e., higher-period regions) potentially cause side effects on structural safety.<sup>49</sup> This is also why a smaller starting frequency of 0.06 Hz is recommended when no specific structures are involved. In this situation, the correlation analysis may not be the optimal result; however, the energy-frequency parameter still strongly correlates with EDP. More data in Figure S6 also reveal this phenomenon. In addition, the ending frequency has less influences on energy-frequency parameters but is set to 15 Hz considering the frequency range of natural ground motions.

we also test the effects of frequency resolution on energy-frequency parameter. Results in Figure 4D indicate that the correlation coefficient slightly decrease with increasing of frequency resolution ( $\Delta f$ ). The similar results also show in Figure S7. Hence, due to the advantages of HHT on adaptive property and the greater resolution in the low-frequency region than FT and WPT, the HHT frequency-domain energy distribution with frequency resolution of 0.02 and summation range from  $0.3/\alpha$  to 15 Hz is recommend for calculating energy-frequency parameter.

### 4.3 | Comparison with other IMs

The correlation analysis is conducted to compare the proposed energy-frequency parameter with twenty common IMs. Details of the selected IMs are shown in Figure 5, where  $T_m$ ,  $T_o$ , and  $T_{avg}$  are defined in Rathje et al.,<sup>14</sup>  $T_g$  is defined in

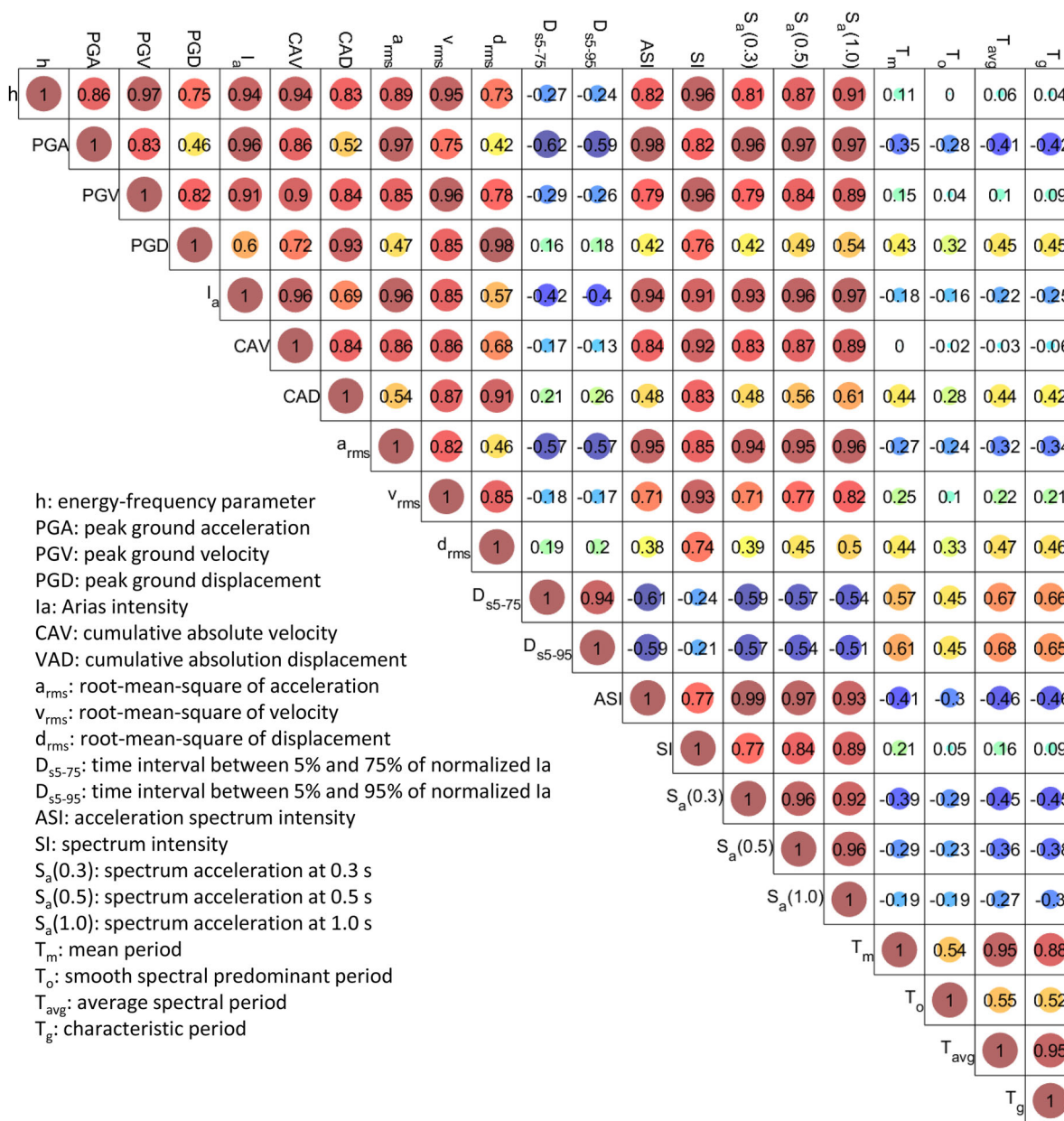


FIGURE 5 Pearson correlation coefficient matrix among IMs

Yang et al.,<sup>15</sup> and the definition and expression of other IMs (including PGA, PGV, PGD,  $I_a$ , CAV, CAD,  $a_{rms}$ ,  $v_{rms}$ ,  $d_{rms}$ ,  $D_{s5-75}$ ,  $D_{s5-95}$ , ASI, SI,  $S_a(T)$ ) could be found in Table 1.

Apart from the data used in nonlinear dynamic analysis in Section 3, more earthquake ground motions in PEER are selected to perform the correlation analysis among the IMs. Totally 9693 ground motions are used herein, and their information is listed in Data S1.

Figure 5 illustrates the Pearson correlation coefficient matrix (see Equation (12)) among IMs at natural logarithm, where the natural logarithm form is adopted because the energy-frequency parameter obeys the lognormal distribution (see Figure S8). Figure 5 indicates that the proposed energy-frequency parameter correlates well with common IMs except for duration- and period-related IMs. This strong correlation ensures that the energy-frequency parameter is of potentially wide applicability in seismic risk analysis. For example, the phenomenon in Figure 2 that the energy-frequency parameter closely relates to the maximum inter-storey drift of structures with different fundamental periods may result from the significant association of  $h$  with PGA, PGV, and PGD.

## 5 | CONCLUSIONS

A novel energy-frequency parameter is proposed for ground motion IM using Hilbert-Huang transform. The proposed parameter is strongly correlated to the EDP for structures with various structural fundamental periods, and verified to be an applicable IM for both ordinary and near-fault pulse-like ground motion in seismic risk analysis. Furthermore, the energy-frequency parameter-based fragility function can be described by a lognormal cumulative distribution function, which helps to facilitate the application of the parameter in seismic risk analysis.

The comparison with other IMs shows that the energy-frequency parameter closely correlates with PGA, PGV, PGD, amplitude-based energy parameter and response spectrum-based IMs. Hence, the proposed IM is of potentially wide applicability in seismic risk analysis. Besides, compared with response spectrum-based IM that is widely considered in seismic structural analysis, the proposed parameter only depends on the ground motion record itself. Hence, the parameter may be more closely related to seismological theory. The relationship between the energy-frequency parameter and seismological parameters (e.g., magnitude and distance) will be carried out in future study.

### ACKNOWLEDGMENTS

This research is supported by the International Joint Research Platform Seed Fund Program of Wuhan University (Grant No. WHUZZJJ202207) and National Natural Science Foundation of China (Grant No. 52079099). Guan Chen would like to thank the financial support of Sino-German (CSC-DAAD) Postdoc Scholarship Program.

### CONFLICT OF INTEREST

The authors declare no potential conflict of interests.

### DATA AVAILABILITY STATEMENT

The raw earthquake ground motions used in the study can be freely downloaded at PEER NGA-West2 database (<https://ngawest2.berkeley.edu/>). Specifically, the ground motion is accessible by searching the earthquake names in the 'Event Name' text box. The processed data are available in the online Supporting Information.

### ORCID

Guan Chen  <https://orcid.org/0000-0002-3709-1247>

Yong Liu  <https://orcid.org/0000-0003-1006-7842>

Takeshi Kitahara  <https://orcid.org/0000-0001-7063-5122>

### REFERENCES

- Porter K. An overview of PEER's performance-based earthquake engineering methodology. In: *9th International Conference on Applications of Statistics and Probability in Civil Engineering*; 2003:1-8.
- Moehle J, Deierlein GG. A framework methodology for performance-based earthquake engineering. In: *13th World Conference on Earthquake Engineering*; 2004.
- Rodgers AJ, Pitarka A, Petersson NA, Sjögreen B, McCallen DB. Broadband (0–4 Hz) ground motions for a magnitude 7.0 Hayward fault earthquake with three-dimensional structure and topography. *Geophys Res Lett*. 2018;45(2):739-747.
- Park J, Bazzurro P, Baker JW. Modeling spatial correlation of groundmotion intensity measures for regional seismic hazard and portfolio loss estimation. In: *Proceeding of the 10th International Conference on Applications of Statistics and Probability in Civil Engineering*. Tokyo, Japan, 31 July–3 August 2007.
- De Biasio M, Grange S, Dufour F, Allain F, Petre-Lazar I. A simple and efficient intensity measure to account for nonlinear structural behavior. *Earthquake Spectra*. 2014;30(4):1403-1426.
- Danciu L, Tselentis GA. Engineering ground-motion parameters attenuation relationships for Greece. *Bull Seismol Soc Am*. 2007;97(1B):162-183.
- Sarma S. Energy flux of strong earthquakes. *Tectonophysics*. 1971;11(3):159-173.
- Trifunac MD, Brady AG. A study on the duration of strong earthquake ground motion. *Bull Seismol Soc Am*. 1975;65(3):581-626.
- Bommer JJ, Martinez-Pereira A. The effective duration of earthquake strong motion. *J Earthquake Eng*. 1999;3(02):127-172.
- Rathje EM, Abrahamson NA, Bray JD. Simplified frequency content estimates of earthquake ground motions. *J Geotech Geoenviron Eng*. 1998;124(2):150-159.
- Arias A. Measure of earthquake intensity. In: *Proceedings of Seismic Design for Nuclear Power Plants, Cambridge, Massachusetts*. Massachusetts Institute of Technology Press; 1970.



12. Karsan I, Jirsa J. Behavior of concrete under compressive loadings. *J Struct Division*. 1969;95(12):2543-2564.
13. Housner G, Jennings PC. Generation of artificial earthquakes. *J Eng Mechanics Division* 1964;90(1):113-150.
14. Rathje EM, Faraj F, Russell S, Bray JD. Empirical relationships for frequency content parameters of earthquake ground motions. *Earthquake Spectra*. 2004;20(1):119-144.
15. Yang D, Pan J, Li G. Non-structure-specific intensity measure parameters and characteristic period of near-fault ground motions. *Earthquake Eng Struct Dyn*. 2009;38(11):1257-1280.
16. Von Thun JL, Roehm LH, Scott GA, Wilson JA. Earthquake ground motions for design and analysis of dams. In: *Proceedings of Earthquake Engineering and Soil Dynamics II—Recent Advances in Ground-Motion Evaluation*. Park City, Utah, United States, June 27–30, 1988.
17. Kramer SL. *Geotechnical Earthquake Engineering*. Pearson Education India; 1996.
18. Iervolino I, Manfredi G, Cosenza E. Ground motion duration effects on nonlinear seismic response. *Earthquake Eng Struct Dyn*. 2006;35(1):21-38.
19. Bommer JJ, Magenes G, Hancock J, Penazzo P. The influence of strong-motion duration on the seismic response of masonry structures. *Bull Earthquake Eng*. 2004;2(1):1-26.
20. Mori Y, Furukawa T. Probabilistic predictor of seismic demand on SMRF based on natural-period-dependent spectrum intensity. *Struct Saf*. 2021;89:102040.
21. Trifunac MD. Earthquake response spectra for performance based design – a critical review. *Soil Dyn Earthquake Eng*. 2012;37:73-83.
22. Bojórquez E, Iervolino I. Spectral shape proxies and nonlinear structural response. *Soil Dyn Earthquake Eng*. 2011;31(7):996-1008.
23. Baker JW, Cornell AC. A vector-valued ground motion intensity measure consisting of spectral acceleration and epsilon. *Earthquake Eng Struct Dyn*. 2005;34(10):1193-1217.
24. Kohrangi M, Vamvatsikos D, Bazzurro P. Pulse-like versus non-pulse-like ground motion records: spectral shape comparisons and record selection strategies. *Earthquake Eng Struct Dyn*. 2019;48(1):46-64.
25. Bora SS, Scherbaum F, Kuehn N, Stafford P. On the relationship between Fourier and response spectra: implications for the adjustment of empirical ground-motion prediction equations (GMPEs). *Bull Seismol Soc Am*. 2016;106(3):1235-1253.
26. Mollaioli F, Bruno S, Decanini L, Saragoni R. Correlations between energy and displacement demands for performance-based seismic engineering. *Pure Appl Geophys*. 2011;168(1):237-259.
27. Decanini LD, Mollaioli F. An energy-based methodology for the assessment of seismic demand. *Soil Dyn Earthquake Eng*. 2001;21(2):113-137.
28. Uang CM, Bertero VV. Evaluation of seismic energy in structures. *Earthquake Eng Struct Dyn*. 1990;19(1):77-90.
29. Sucuoğlu H, Nurtuğ A. Earthquake ground motion characteristics and seismic energy dissipation. *Earthquake Eng Struct Dyn*. 1995;24(9):1195-1213.
30. Benedetti D, Carydis P, Limongelli M. Evaluation of the seismic response of masonry buildings based on energy functions. *Earthquake Eng Struct Dyn*. 2001;30(7):1061-1081.
31. Manfredi G. Evaluation of seismic energy demand. *Earthquake Eng Struct Dyn*. 2001;30(4):485-499.
32. Wu Q, Li DQ, Du W. Identification of optimal ground-motion intensity measures for assessing liquefaction triggering and lateral displacement of liquefiable sloping grounds. *Earthquake Spectra*. 2022;87552930221094344.
33. Hu J, Lai Q, Liu B, Xie L. Ranking of ground motions destructive capacity for low-and middle-rise RC frame structures based on a comprehensive intensity measure. *Adv Struct Eng* 2022:13694332211072319.
34. Tothong P, Cornell CA. Structural performance assessment under near-source pulse-like ground motions using advanced ground motion intensity measures. *Earthquake Eng Struct Dyn*. 2008;37(7):1013-1037.
35. Huang NE, Shen Z, Long SR, et al. The empirical mode decomposition and the Hilbert spectrum for nonlinear and non-stationary time series analysis. *Proc R Soc London. Series A: Mathematical, Physical and Engineering Sciences* 1998;454(1971):903-995.
36. Ancheta TD, Darragh RB, Stewart JP, et al. NGA-West2 database. *Earthquake Spectra*. 2014;30(3):989-1005.
37. Chen G, Beer M, Liu Y. Modeling response spectrum compatible pulse-like ground motion. *Mech Syst Sig Process*. 2022;177:109177.
38. Phan V, Saiidi MS, Anderson J, Ghasemi H. Near-fault ground motion effects on reinforced concrete bridge columns. *J Struct Eng*. 2007;133(7):982-989.
39. Chen G, Beer M, Liu Y. Identification of near-fault multi-pulse groundmotion, under review.
40. Baker JW. Quantitative classification of near-fault ground motions using wavelet analysis. *Bull Seismol Soc Am*. 2007;97(5):1486-1501.
41. Scott B, Park R, Priestley M. Stress-strain behavior of concrete confined by overlapping hoops at low and high strain rates. *J Am Concrete Inst* 1982;79(1):13-27.
42. Luco N, Cornell CA. Structure-specific scalar intensity measures for near-source and ordinary earthquake ground motions. *Earthquake Spectra* 2007;23(2):357-392.
43. Suzuki A, Iervolino I. Seismic fragility of code-conforming Italian buildings based on SDoF approximation. *J Earthquake Eng*. 2021;25(14):2873-2907.
44. Cornell CA, Jalayer F, Hamburger RO, Foutch DA. Probabilistic basis for 2000 SAC federal emergency management agency steel moment frame guidelines. *J Struct Eng*. 2002;128(4):526-533.
45. Eads L, Miranda E, Krawinkler H, Lignos DG. An efficient method for estimating the collapse risk of structures in seismic regions. *Earthquake Eng Struct Dyn*. 2013;42(1):25-41.



46. Porter K, Kennedy R, Bachman R. Creating fragility functions for performance-based earthquake engineering. *Earthquake Spectra* 2007;23(2):471-489.
47. Li QY, Chen G, Luo DY, Ma HP, Liu Y. An experimental study of a novel liquid carbon dioxide rock-breaking technology. *Int J Rock Mech Min Sci*. 2020;128:104244.
48. Chen G, Li QY, Li DQ, Wu ZY, Liu Y. Main frequency band of blast vibration signal based on wavelet packet transform. *Appl Math Modell*. 2019;74:569-585.
49. Baker JW, Cornell AC. Spectral shape, epsilon and record selection. *Earthquake Eng Struct Dyn*. 2006;35(9):1077-1095.

## SUPPORTING INFORMATION

Additional supporting information can be found online in the Supporting Information section at the end of this article.

**How to cite this article:** Chen G, Yang J, Liu Y, Kitahara T, Beer M. An energy-frequency parameter for earthquake ground motion intensity measure. *Earthquake Engng Struct Dyn*. 2023;52:271–284.  
<https://doi.org/10.1002/eqe.3752>